REGULAR PAPER

Particle-in-cell Monte Carlo collision simulation and experimental measurement of Ar plasma in a fast atom beam source for surface-activated bonding

Japanese Journal of Applied Physics **60**, SCCB01 (2021) **REGULAR PAPER**
https://doi.org/**10.35848/1347-4065/abe683**

Particle-in-cell Monte Carlo collision simulation and experimental measurement of Ar plasma in a fast atom beam source for surface-activated bonding

Ryo Morisaki[1], Takahiro Yamazaki[1], Chiemi Oka[1], Junpei Sakurai[1], Takami Hirai[2], Tomonori Takahashi[2], Hiroyuki Tsuji[2], Noriyasu Ohno[3], and Seiichi Hata[1*]

[1]*Department of Micro-Nano Mechanical Science and Engineering, Graduate School of Engineering, Nagoya University, Furo-cho, Chikusa-ku, Nagoya, Aichi 464-8601, Japan*
[2]*NGK INSULATORS, Ltd., 2-56 Suda-cho, Mizuho-ku, Nagoya, Aichi 467-8530, Japan*
[3]*Department of Electrical Engineering, Graduate School of Engineering, Nagoya University, Furo-cho, Chikusa-ku, Nagoya, Aichi 464-8601, Japan*

[*]E-mail: seiichi.hata@mae.nagoya-u.ac.jp

Received November 30, 2020; revised January 20, 2021; accepted February 15, 2021; published online March 2, 2021

Ar plasma in a fast atom beam (FAB) source with magnetic fields, which was previously developed [Precis. Eng. **62**, 106 (2020)] to achieve high-performance surface activated bonding, was analyzed by particle-in-cell-Monte Carlo collision simulation and experimental measurements. Simulation in the proposed FAB source with magnetic fields shows that higher electron density accumulation occurs near the irradiation port by $E \times B$ drift, and the potential gradient near the irradiation port steepens, which results in an increase in Ar^+ flux to the irradiation port. The variation in the plasma distribution due to the effect of the magnetic field contributes to an increase in the amount of Ar-FAB irradiation, which reduces erosion of the carbon electrodes and suppresses the formation of carbon agglomerates. These simulation results were verified experimentally with Langmuir probe measurements and FAB irradiation experiments with oxide layer removal. The analysis results explain why high performance is achieved with the proposed FAB source. © 2021 The Japan Society of Applied Physics

1. Introduction

The surface-activated bonding (SAB) process is a room-temperature bonding method that does not require an intermediate layer.[1–4] The surfaces of wafers are cleaned and activated by fast atom beam (FAB) irradiation under vacuum. After the irradiation, the wafers are brought into contact. The interface is an amorphous layer that enhances the bonding strength to as much as that in the bulk materials.[1,3] Ar plasma is generated in a FAB source in the SAB process. In the conventional FAB source, plasma potential distribution is formed like a saddle.[5] Electrons are induced to oscillate between two cathodes under the action of the saddle field.[6] Electrons emitted from a cathode move to a high potential area, reach the opposite cathode through a saddle point which is located at the center of two anodes, and return to the opposite cathode.[6] The electrons which have long trajectories cause to generate plasma stably and efficiency like a hollow cathode discharge.[7]

It is a matter for SAB that the lifetime of the FAB source is short. After repeated use, the inner carbon electrodes of the FAB source are eroded by Ar^+ sputtering, carbon abrasion powders are generated, agglomerated, and then attach to the interface of the wafers. Therefore, we have proposed a novel FAB source as a countermeasure.[8] The lifetime of the proposed source is 5 times as long as that of the conventional source. In addition, the proposed source has 15 times the Ar-FAB irradiation efficiency of the conventional source.

In the proposed FAB source, electrons are guided to the irradiation port by the applied magnetic field and Ar^+ ions follow the electrons. It was reported that the accumulation of high-density Ar plasma near the irradiation port caused a reduction in Ar^+ sputtering and abrasion of the source, which improves the Ar-FAB irradiation efficiency.[8] However, details of the plasma characteristics in the proposed source have yet to be clarified. In this study, we analyzed Ar plasma in the proposed FAB source by particle-in-cell-Monte Carlo collision (PIC-MCC) simulation. The distribution of electrons, Ar^+ ions, the plasma potential, and the Ar^+ flux in the source are simulated to research the cause of the improved performance with the proposed FAB source. The simulation results were verified experimentally using a single Langmuir probe[9–12] and FAB irradiation experiments with oxide layer removal.[8]

2. Experimental methods

The PEGASUS simulation software[13–17] with a PIC-MCC module was used in this work. The PIC and MCC methods were used to analyze electromagnetic fields, the motion of charged particles, and collisions of ions, electrons, and neutrals in a plasma.[13–17] Figure 1 shows a schematic diagram of the electrodes and the magnetic flux density distributions in the source. In the proposed FAB source, magnetic fields are applied by permanent magnets and yokes. Some parts of the yokes are inside the source. The yokes do not prevent the plasma generation in the source because they are covered by carbon thin plates and are grounded. The source has a cooling mechanism for cooling the yokes and permanent magnets which are heated by plasma exposure and heat conduction. The surface temperature of magnets is confirmed lower than 333 K by thermo-labels. The simulation of the proposed FAB source is two-dimensional. The simulated system is a cross section of the source not including yokes (B-B′ section) and whose size is 63.5×53.5 mm. The Ar gas pressure inside the source is 10 Pa. The cathode walls are grounded. Anodes with a diameter of 10 mm are biased at +500 V. In this study, the plasma was analyzed while varying the distance a (between the anodes, $a = 3$, 18, 33 mm) with magnetic fields (i), (ii), (iii), or without a magnet field. It is assumed that the distance a and applying magnetic field affect the plasma generation and transportation, respectively. The aperture for Ar-FAB irradiation was not considered in the simulation. Table I shows the chemical reactions in the simulated Ar discharges.

Langmuir probe measurements[9–12] and irradiation experiments with oxide layer removal[8] were performed. The

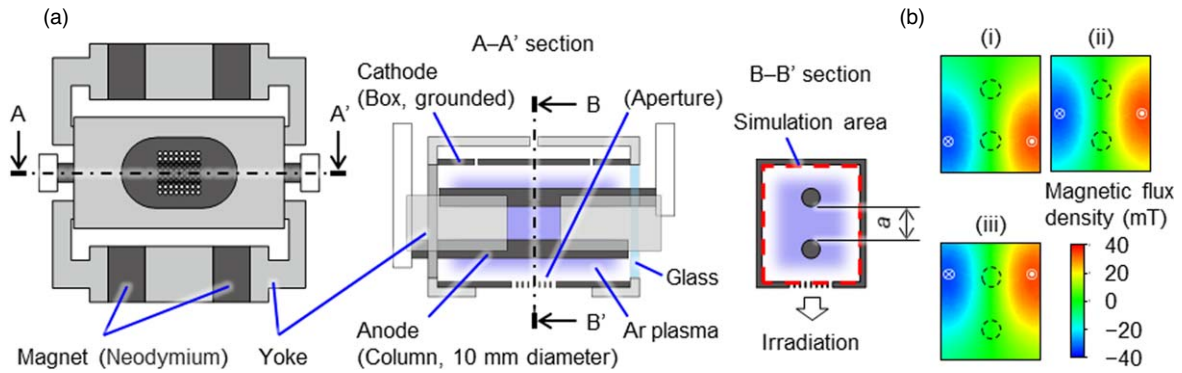

Fig. 1. (Color online) (a) Schematic illustrations of the electrodes and (b) magnetic flux density distributions with various magnetic fields obtained by simulation of the proposed FAB source. The plasma state in the source could be observed through the glass window.

Table I. Chemical reactions for Ar discharge.

Reaction	Formula
1	$e^- + e^- \rightarrow e^- + e^-$
2	$e^- + Ar \rightarrow Ar + e^-$
3	$e^- + Ar \rightarrow Ar^+ + e^- + e^-$
4	$e^- + Ar \rightarrow Ar^* + e^-$
5	$Ar^+ + Ar \rightarrow Ar + Ar^+$
6	$Ar^+ + Ar \rightarrow Ar^+ + Ar$
7	$e^- + Ar^+ \rightarrow Ar$
8	$Ar^* \rightarrow Ar$

proposed FAB source was set in the vacuum chamber. The internal and external pressures for the FAB source were measured. DC discharge power was supplied to the FAB source to control the discharge current. A mass flow controller was used to regulate the Ar gas flow rate into the FAB source from 0 to 1.67 $m^3\ s^{-1}$ (100 sccm).

The Langmuir probe was used to measure the electron density distribution (n_e), electron temperature (T_e), and plasma potential (V_s). Figure 2 shows the measurement circuit. The probe bias voltages, which are DC and AC, were applied from a function generator and bipolar power supply. Current–voltage (I_p–V_p) characteristics were obtained by measurement of V_1 and V_2 and the n_e, T_e, and V_s plasma parameters were calculated based on the I_p–V_p characteristics. Irradiation experiments were conducted to evaluate the amount of Ar-FAB irradiation in terms of oxide layer removal. The Ar-FAB irradiated a Si wafer with an oxide layer. The amount of SiO_2 removal was measured by optical interference. The etching rate obtained was then evaluated by dividing the volume of SiO_2 removed by the irradiation time.

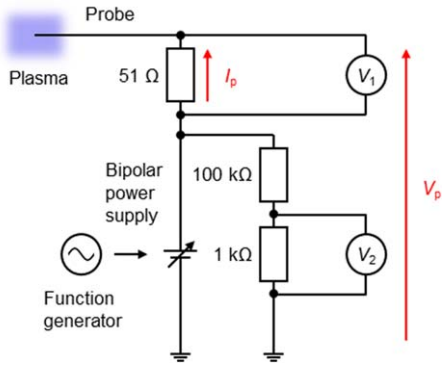

Fig. 2. (Color online) Schematic illustration of the measurement circuit for the Langmuir probe study.

3. Results and discussion

3.1. PIC-MCC simulation

PIC-MCC simulation of the proposed FAB source suggests the densification of electrons and Ar^+ ions near the irradiation port by application of a magnetic field. Figure 3(a) shows electron density distributions in the source, with and without a magnetic field. Without a magnetic field, the electrons are distributed mainly around the anodes. In contrast, when a magnetic field is applied, a higher density distribution of electrons is formed near the irradiation port by $E \times B$ motion not depending on a positive or a negative charge. The electron density is higher with mag. (i) which forms the higher magnetic flux density near the irradiation port. With mag. (i), higher electron density distribution is formed at the center of the FAB source where is the lower magnetic flux density. In contrast, with mag. (iii), lower magnetic flux density near the irradiation port has a smaller influence on plasma transportation to the port and forms lower electron density. A similar tendency is also observed in the density distribution of Ar^+. Figure 3(b) shows the experimentally observed two-dimensional distribution of visible light emission from the argon plasma, which corresponds to Fig. 3(a) with mag. (i). The visible light emission from the argon plasma is observed to move downward due to the effect of the magnetic field. The visible emission intensity observed in the experiment is a line integral value and is not directly proportional to the electron density, although the experiment and simulation are in good qualitative agreement with respect to the change in the plasma distribution. These results support the proposed physical mechanism to achieve high-performance with the FAB source developed in the previous study.[8)]

The calculated plasma potential for the proposed FAB source shows that a steep potential gradient is formed near the irradiation port by the application of a magnetic field. Figure 4 shows the plasma potential distribution in the source. The positively biased anode (+500 V) determines the plasma potential in the bulk region. An ion sheath is formed in front of the grounded cathode wall. Without a magnetic field, the ion sheath thickness is uniform along the cathode wall because the electron density near the cathode is almost the same over the entire region, as shown in Fig. 3(a). In contrast, by applying magnetic fields, the ion sheath thickness becomes smaller in the bottom region in relation to the accumulation of electrons as shown in Fig. 3(a). A

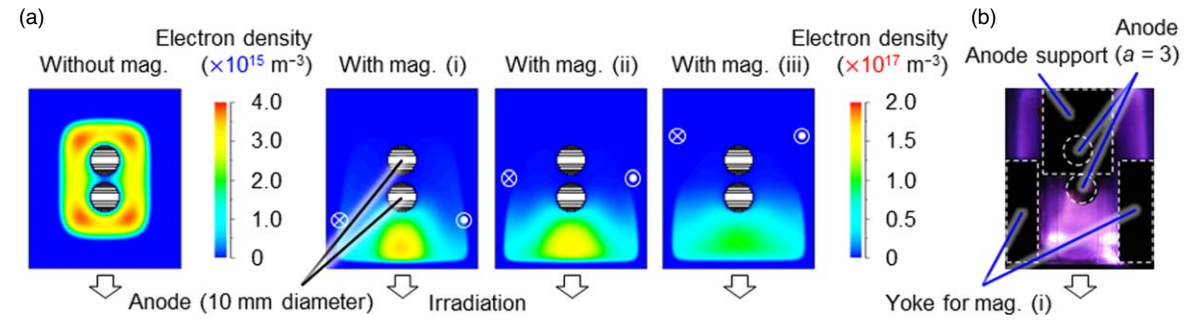

Fig. 3. (Color online) (a) Distributions of electron density in the proposed FAB source with and without a magnetic field ($a = 3$ mm). (b) The plasma state in the proposed FAB source (with mag. (i), $a = 3$ mm).

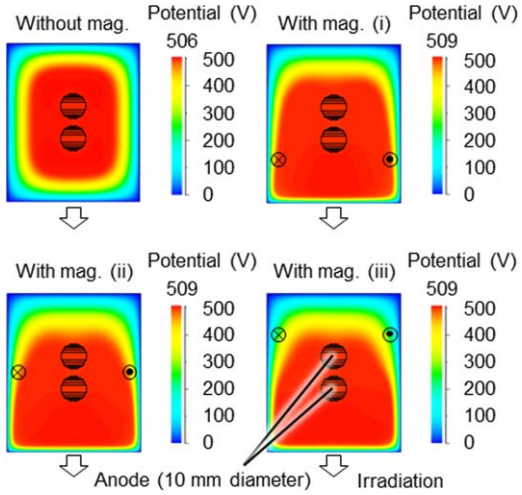

Fig. 4. (Color online) Plasma potentials in the proposed FAB source with and without a magnetic field ($a = 3$ mm).

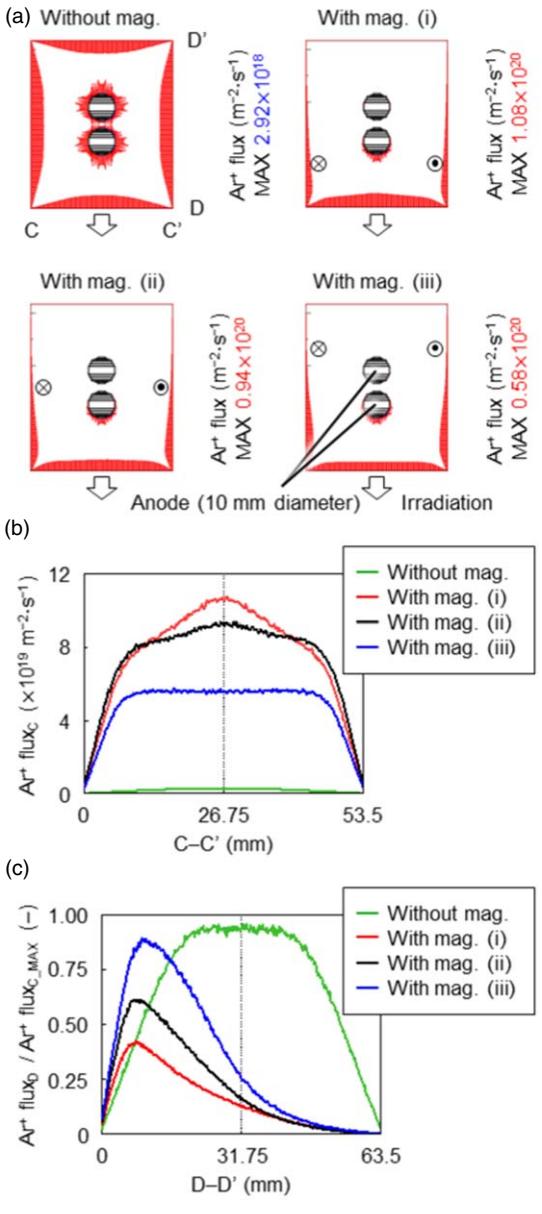

Fig. 5. (Color online) (a) Distributions of the Ar^+ wall flux in the proposed FAB source with and without a magnetic field. (b) Ar^+ flux to the C-C′ wall (irradiation port). (c) The ratio of Ar^+ flux to the D-D′ wall with respect to the maximum of Ar^+ flux to the C-C′ wall.

smaller ion sheath thickness indicates that a steeper potential gradient is formed near the irradiation port. This steep potential gradient reduces the collision of Ar^+ ions with neutral Ar in the ion sheath and enables efficient acceleration of Ar^+ ions toward the irradiation port.

The application of a magnetic field enhances the Ar^+ flux to the lower wall with the irradiation port, which results in a relative reduction of the Ar^+ flux to the other walls. Figure 5(a) shows the distribution of the Ar^+ flux to the walls. The height of the red bars indicates the Ar^+ flux intensity. Note that the scale of the bar height is different with and without a magnetic field. Without a magnetic field, the Ar^+ flux is entirely distributed to all walls and takes a maximum value at the center of each wall. In contrast, with a magnetic field, a high density of Ar^+ ions is accumulated near the lower wall and is accelerated toward the lower wall (C-C′ wall) due to the steep potential gradient in the narrow ion sheath, which results in a large Ar^+ flux intensity, as shown in Fig. 5(b). Further, the Ar^+ flux onto the other walls [e.g. the D-D′ wall as shown in Fig. 5(c)] decreases relatively in association with the reduction in the Ar^+ density near the walls. This result suggests a decrease in the total erosion of the carbon walls (cathode electrodes) due to Ar^+ sputtering in the proposed FAB source, which leads to fewer carbon agglomerates from the walls. This simulation result is consistent with the experimental observation of the previous study,[8] in which less wear was observed on the electrodes of the proposed FAB source, even after long time use. The lifetime of the proposed FAB source is 5 times as long as that of a conventional FAB source. Accelerated Ar^+ toward the irradiation port is irradiated as Ar-FAB after being neutralized by charge exchange and surface recombination processes. Stronger Ar-FAB irradiation of the proposed FAB

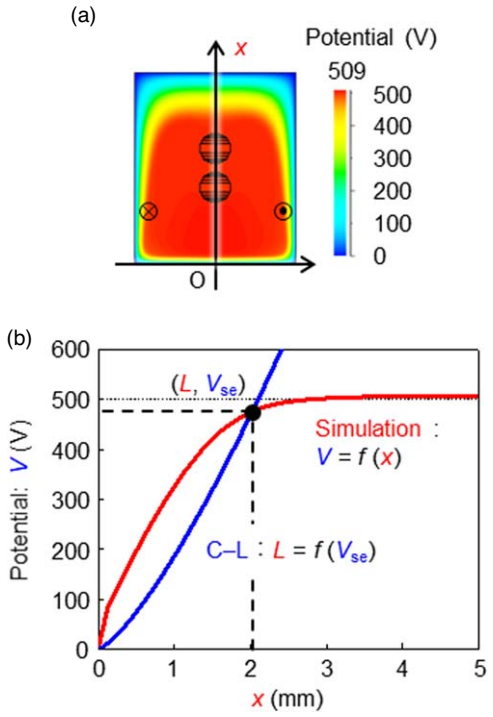

Fig. 6. (Color online) (a) Plasma potential distribution and (b) thickness of the ion sheath obtained by simulation results in (a) using the Child–Langmuir (C–L) law with mag. (i) ($a = 3$ mm).

source is realized over that of a conventional FAB source. In the next section, these simulation results are verified experimentally.

These simulation results also show that the proposed FAB source achieves high-energy Ar-FAB irradiation due to less ion-neutral collisions in the ion sheath. The thickness of the ion sheath in the source was evaluated to clarify the factors that influence the high performance of the proposed FAB source. The mean thickness of the ion sheath in front of the irradiation port (C-C′ wall) was calculated based on the Ar^+ flux to the wall and the plasma potential using the Child–Langmuir law:[18–20)]

$$j = \frac{4}{9}\varepsilon_0\sqrt{\frac{2e}{m}}\frac{V^{3/2}}{L^2}, \tag{1}$$

where j is the current density, ε_0 is the permittivity of free space, e and m are respectively the charge and mass of the Ar^+ ions, V is the potential at the sheath edge, and L is the thickness of the ion sheath. The current density j to the irradiation port (C-C′ wall) is calculated from the results for the Ar^+ flux distribution. The potential at the ion sheath edge V is obtained from the plasma potential on the centerline of the FAB source (Fig. 6). Figure 6 shows the thickness of the ion sheath determined by the intersection of curves obtained by the Child–Langmuir law and the plasma potential profile in the simulation. Figure 7 shows the thickness of the ion sheath under various conditions. The effect of the applying magnetic field on the plasma state in the source is larger than that of the distance a. When a magnetic field is applied, the thickness of the ion sheath is smaller than that without a magnetic field. A steep potential gradient is formed near the irradiation port in the proposed FAB source. The mean free path length λ of Ar^+ collided with neutrals (Ar) is calculated using Eq. (2):

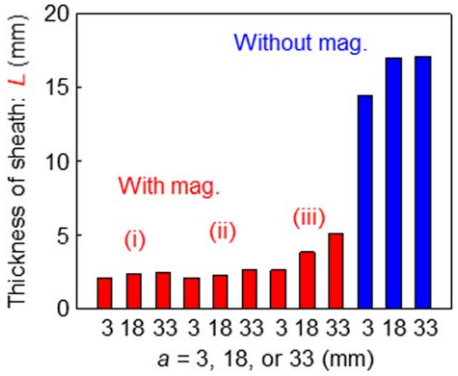

Fig. 7. (Color online) Thickness of the ion sheath under various conditions estimated using the Child–Langmuir law and plasma potential simulations.

$$\lambda = \frac{1}{\sigma n}, \tag{2}$$

where σ is the collisional cross section between Ar^+ and Ar, and n is the Ar density. λ is estimated to be ca. 3 mm with an Ar pressure of 4 Pa under the experimental condition, which is almost the same as the estimated thickness of the ion sheath (2.1–5.1 mm). This indicates that sufficient acceleration of Ar^+ enables the generation of high-energy Ar^+ beams. This high-energy Ar^+ beam is considered to be neutralized by the charge exchange process in the ion sheath or between the FAB source and the bonding wafer (typical distance of ca. 100 mm), which prevents charge-up damage to the bonding wafer.

3.2. Experimental measurements

Experimental measurements have confirmed the validity of the simulation results. There are some differences between the simulation and experimental conditions, such as the pressure in the source and the voltage applied to the anodes. In the simulations, the Ar pressure was higher than that in the experiments to improve the convergence of the calculations. In the experiments, the voltage applied to the anodes was not fixed due to the current control system. However, the results of the simulations and experimental measurements can be compared and evaluated qualitatively.

The electron density (n_e) profiles measured with a Langmuir probe in the proposed FAB source agreed with the simulation qualitatively. The Langmuir probe measurement was conducted at positions I, II, and III shown in Fig. 8(a). Figure 8(b) shows the dependence of n_e on the discharge electric current measured at positions I, II, and III. n_e increased with the discharge electric current, and was a maximum at position II and a minimum at position III. This tendency is consistent with the simulation results shown in Fig. 8(c). Figure 9 shows n_e measured at point II for various Ar pressures. The Ar pressure was varied from 3.4 to 4.6 Pa by controlling the experimental Ar gas flow rate from 70 to 100 sccm. A higher n_e was measured at a higher Ar pressure under the condition where the discharge electric current was the same. Assuming n_e changes linearly with respect to the Ar pressure, the extrapolated experimental results are close to the simulations, and the validity of the simulation is confirmed.

Measurements of the amount of Ar-FAB irradiation by irradiation experiments were also consistent with the simulated results, excluding the condition for the application of a

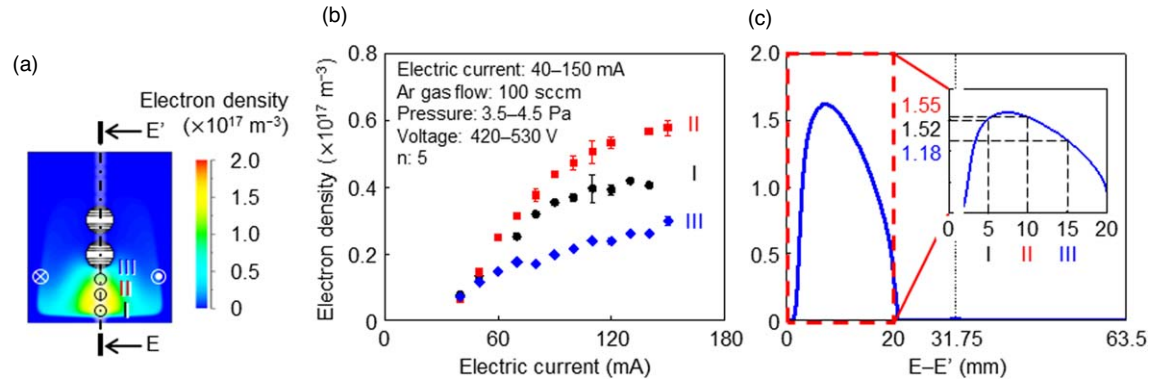

Fig. 8. (Color online) (a) Measurement points (I–III) for the Langmuir probe study, (b) experimental electron density distributions under different current conditions, and (c) simulated electron density distributions.

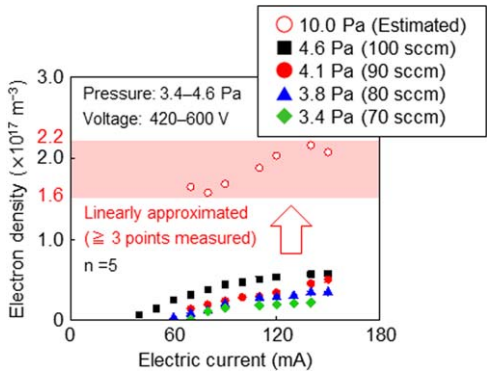

Fig. 9. (Color online) Electron density measured at point II under various inner pressure conditions obtained by changing the Ar gas inflow and estimated value assuming linear change with respect to the inner pressure.

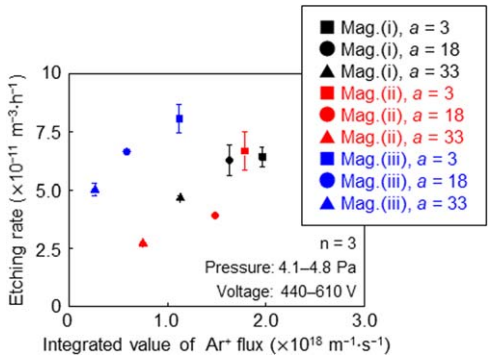

Fig. 10. (Color online) Comparison of the simulation results (the integrated value of Ar^+ flux to the irradiation port of the aperture section) and experimental results (etching rate) under various conditions.

magnetic field (iii). Irradiation experiments were conducted with various positions of the anodes and the magnetic field to evaluate the etching rate. Simulations were also performed with various conditions and the integrated value of the Ar^+ flux to the irradiation port of the aperture section was evaluated. Figure 10 shows the integrated value of Ar^+ flux to the irradiation port of the aperture section (simulation results) versus the etching rate (experimental results). The amount of Ar-FAB irradiation for the experiments and simulations was in good agreement, except for the condition with application of a magnetic field (iii). These results also indicate that the Ar-FAB irradiation efficiency with the proposed FAB source was improved by an increase of the Ar^+ density and formation of a steep potential gradient near the irradiation port. Moreover, the relative decrease of the Ar^+ flux, except to the irradiation port, showed that wear on the carbon walls was suppressed and the proposed FAB source achieved a longer lifetime. We consider that the cause of the discordance between the experiments and simulations was due to simulation conditions such as the Ar gas flow and the decrease in the magnetic field strength after long use. In this study, the Ar gas pressure was uniformly distributed in the simulated system. Considering the Ar gas flow, the simulation can reproduce the initial Ar density distribution in the FAB source. Moreover, the amount of Ar-FAB irradiation of the wafer could be evaluated directly. The yokes for applying a magnetic field in the proposed FAB source are heated by plasma exposure. It is assumed that the magnetic field strength decreases due to this heating after long-time use, which leads to a difference in the control of the charged particles caused by an increase of the Larmor radius. In the simulation, the magnetic flux density distribution before use was adopted. To resolve this mismatch, it is necessary to consider the Ar gas flow inside and outside the FAB source and the temporal change of the magnetic field strength caused by exposure to the plasma and heating.

4. Conclusions

Ar plasma in the proposed FAB source was analyzed by PIC-MCC simulations and the factor by which the source achieved a higher efficiency of Ar-FAB irradiation, i.e. the suppression of Ar^+ sputtering, which led to less wear inside the source, was clarified. The simulation results were verified experimentally using a single Langmuir probe and FAB irradiation experiments. In the proposed FAB source with a magnetic field, a higher density distribution of electrons was formed near the irradiation port by $E \times B$ motion, and a steep plasma potential gradient was formed near the irradiation port, which resulted in an enhanced Ar^+ flux to the irradiation port and a relative reduction of the Ar^+ flux to the other walls. The simulation results also show that the proposed FAB source achieves high-energy Ar-FAB irradiation due to less ion-neutral collisions in the ion sheath and a reduction of carbon agglomerates from the electrodes due to Ar^+ sputtering.

In future work, we plan to develop a higher-performance FAB source with consideration of these simulation results. Moreover, to improve the accuracy of plasma analysis, we will conduct comprehensive plasma simulations that include

a wafer to be irradiated by Ar-FAB, a chamber, and Ar gas flow internal and external to the FAB source. In addition, we will replace the permanent magnet with an electromagnet for the application of a magnetic field in the proposed FAB source to prevent the decrease in magnetic field strength.

ORCID iDs

Takahiro Yamazaki https://orcid.org/0000-0003-0738-9373

1) H. Takagi, K. Kikuchi, R. Maeda, T. R. Chung, and T. Suga, Appl. Phys. Lett. **68**, 2222 (1996).
2) H. Takagi, R. Maeda, N. Hosoda, and T. Suga, Jpn. J. Appl. Phys. **38**, 1589 (1999).
3) E. Higurashi, Y. Sasaki, R. Kurashima, T. Suga, Y. Doi, Y. Sawayama, and I. Hosako, Jpn. J. Appl. Phys. **54**, 030213 (2015).
4) H. Takagi, Y. Kurashima, A. Takamizawa, T. Ikegami, and S. Yanagimachi, Jpn. J. Appl. Phys. **57**, 02BA04 (2018).
5) D. Sarangi, O. S. Panwar, S. Kumar, and R. Bhattacharyya, Vacuum **58**, 609 (2000).
6) J. Franks, Vacuum **34**, 259 (1984).
7) P. F. Little and A. Von Engel, Proc. R. Soc. A **224**, 209 (1954).
8) R. Morisaki, Y. Hirai, C. Oka, M. Mizoshiri, T. Yamazaki, J. Sakurai, T. Hirai, T. Takahashi, H. Tsuji, and S. Hata, Precis. Eng. **62**, 106 (2020).
9) S. Bhattarai and L. N. Mishra, Int. J. Phys. **5**, 73 (2017).
10) I. Langmuir, Science **58**, 290 (1923).
11) H. M. M. Smith and I. Langmuir, Phys. Rev. **28**, 727 (1926).
12) V. A. Godyak and V. I. Demidov, J. Phys. D **44**, 233001 (2011).
13) Y. Miyagawa, M. Ikeyama, S. Miyagawa, and H. Nakadate, Nucl. Instrum. Methods Phys. Res. B **206**, 767 (2003).
14) Y. Miyagawa, H. Nakadate, M. Tanaka, M. Ikeyama, and S. Miyagawa, Surf. Coat. Technol. **196**, 155 (2005).
15) Y. Miyagawa, M. Tanaka, M. Ikeyama, S. Nakao, J. Choi, and S. Miyagawa, Nucl. Instrum. Methods Phys. Res. B **242**, 341 (2006).
16) Y. Miyagawa, M. Ikeyama, S. Miyagawa, M. Tanaka, and H. Nakadate, Comput. Phys. Commun. **177**, 84 (2007).
17) M. W. Kunz, J. M. Stone, and X. N. Bai, J. Comput. Phys. **259**, 154 (2014).
18) Y. Li, H. Wang, C. Liu, and J. Sun, Appl. Surf. Sci. **251**, 19 (2005).
19) C. D. Child, Phys. Rev. (Series I) **32**, 492 (1911).
20) I. Langmuir, Phys. Rev. **21**, 419 (1923).